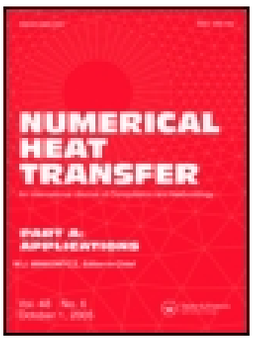

Numerical Heat Transfer

ISSN: 1040-7782 (Print) 1521-0634 (Online) Journal homepage: https://www.tandfonline.com/loi/unht20

CALCULATION OF STEADY AND UNSTEADY FLOWS IN A FILM-COOLING ARRANGEMENT USING A TWO-LAYER ALGEBRAIC STRESS MODEL

L. S. Jansson , L. Davidson & E. Olsson

To cite this article: L. S. Jansson , L. Davidson & E. Olsson (1994) CALCULATION OF STEADY AND UNSTEADY FLOWS IN A FILM-COOLING ARRANGEMENT USING A TWO-LAYER ALGEBRAIC STRESS MODEL, Numerical Heat Transfer, 25:3, 237-258, DOI: 10.1080/10407789408955947

To link to this article: https://doi.org/10.1080/10407789408955947

CALCULATION OF STEADY AND UNSTEADY FLOWS IN A FILM-COOLING ARRANGEMENT USING A TWO-LAYER ALGEBRAIC STRESS MODEL

L. S. Jansson, L. Davidson, and E. Olsson
Department of Thermo and Fluid Dynamics, Chalmers University of Technology, Gothenburg, Sweden

In recent years there has been a growing interest in ceramic materials for high-temperature gas turbine chambers. Owing to different material properties, these gas turbine chambers have thicker walls than the metallic ones and, thus, a different geometry of the film-cooling slots, which affects the flow field. In this work the mean and fluctuating velocities and fluid temperatures have been studied numerically for two different lip-to-slot ratios. When the lip is thick, the flow becomes unsteady and a vortex street appears behind the lip; hence, unsteady computations have been carried out. The calculated results are compared with single hot-wire measurements made recently by Boman [1].

The purpose of this investigation is to model both the flow and temperature fields, numerically, at different slot-lip thicknesses and flow ratios in a two-dimensional slot with tangential injection. The validity of the eddy-viscosity concept and an algebraic stress model are examined. The results are related to the wake flow characteristics downstream of the lip. Launder and Rodi [2] examined how well current calculation schemes succeed in mimicking the measured behavior of turbulent wall jets. They found that the models derived from the Reynolds stress transport equation (whether of a full Reynolds stress model (RSM) or an algebraic stress model (ASM) form) were more successful than the Boussinesq stress-strain relation in imitating the behavior of the wall jets and that a crucial element in these closures is the modeling of turbulent pressure reflections from the wall. It is this process that is responsible for the slower growth rate of the plane wall jet than of the free jet.

In most works in the literature, parabolic solvers have been used. An exception is Kacker [3], who used an elliptic *steady* solver. In the present study when the lip was thick ($t/s = 1.0$), a periodic von Kárman vortex street formed behind the lip, causing the flow field to become unsteady and elliptic. In a review by Rodi [4, 5], calculations with a full RSM, an ASM, and the k-ϵ model were presented for a vortex-shedding flow past a circular cylinder. Their results were in better agreement with the data when RSM or ASM was used. These studies concluded that the assumption of the eddy viscosity as a scalar quantity in the k-ϵ model is invalid, that a Reynolds stress equation model is necessary for a realistic

Received 23 December 1992; accepted 22 April 1993.
Address correspondence to L. S. Jansson, Department of Thermo and Fluid Dynamics, Chalmers University of Technology, S-412 96 Gothenburg, Sweden.

Numerical Heat Transfer, Part A, 25: 237–258, 1994

1040–7782/94 $10.00 + .00

NOMENCLATURE

A_μ	constant in the Norris-Reynolds one-equation model	κ	von Karman constant
f_1	damping function	μ, μ_t	dynamic viscosity (laminar and turbulent, respectively)
k	turbulent kinetic energy	ν	kinematic viscosity (laminar)
l_μ, l_ϵ	turbulent length scales	ρ	fluid density
M	relation between the slot and the free stream	τ	time variable
		τ_{ij}	stress tensor
n	normal distance to the wall	Φ_{ij}	pressure-strain redistribution term
$\mathbf{n}_k$	unit vector normal to the wall	$\langle\rangle$	ensemble average, Eq. (25)
P	static pressure		
P_{ij}	production of Reynolds stresses	**Subscripts**	
P_k	production of turbulent kinetic energy	C	center node
		D	downstream node
Re_n	turbulent Reynolds number	g	free stream
s	slot height	$i+1/2, j$	value at a control volume's east face
t	lip thickness	n	normal direction to the wall
T	mean temperature	s	slot
u'	total turbulent fluctuation, Eq. (22)	t	turbulent
u_i	turbulent fluctuating velocity, Eq. (25)	U	upstream node
		w	wall condition
U_i	Cartesian mean velocity		
$\mathbf{x}_i$	Cartesian spatial coordinate vector	**Superscripts**	
δ_{ij}	Kronecker's delta		
ϵ	dissipation rate	~	periodic fluctuation, Eq. (25)
Θ	adiabatic film-cooling effectiveness $[= (T - T_g)/(T_g - T_s)]$	—	time average, Eq. (25)

simulation of this motion, and that a good numerical resolution in the near-wall region is essential for a realistic simulation of vortex shedding.

The present calculations have been made, comparing two different discretization schemes for the convective terms, using both an ASM, in order to better predict the anisotropy effects of the turbulence, and the standard k-ϵ model. These two models using high Reynolds numbers have been combined with a one-equation model by Norris and Reynolds [6] near the walls in order to account for the viscous effects on the turbulence. The configurations considered are relevant to high-temperature gas turbine chambers (Figure 1).

MEAN FLOW EQUATIONS

In Cartesian tensor notation, the time-averaged conservation equations for an incompressible unsteady flow without body forces can be expressed as follows.

Conservation of mass (continuity equation)

$$\frac{\partial \langle U_i \rangle}{\partial x_i} = 0 \tag{1}$$

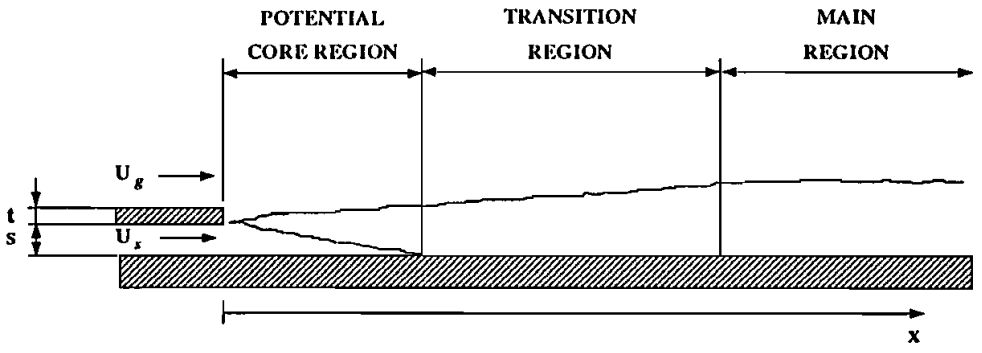

Figure 1. Film model of a two-dimensional wake flow.

Conservation of momentum (transport equation)

$$\frac{\partial}{\partial \tau}\left(\rho\langle U_i\rangle\right) + \frac{\partial}{\partial x_j}\left(\rho\langle U_j\rangle\langle U_i\rangle\right) = -\frac{\partial\langle P\rangle}{\partial x_i} + \frac{\partial \tau_{ij}}{\partial x_j} \tag{2}$$

where the stress tensor τ_{ij} is written as

$$\tau_{ij} = \mu\left(\frac{\partial\langle U_i\rangle}{\partial x_j} + \frac{\partial\langle U_j\rangle}{\partial x_i}\right) - \rho\langle u_i u_j\rangle \tag{3}$$

where, for the unsteady flow case, $\langle U_i\rangle$ denotes the phase average of $\langle U_i\rangle$; see Eq. (25). For the steady flow case, $\langle U_i\rangle = \langle U_i\rangle$, since $\langle U_i\rangle = 0$.

TURBULENCE MODELING

The most common way to model the Reynolds stresses is to use the k-ϵ model, which is based on the eddy viscosity concept according to the Boussinesq assumption:

$$-\rho\langle u_i u_j\rangle = \mu_t\left(\frac{\partial\langle U_i\rangle}{\partial x_j} + \frac{\partial\langle U_j\rangle}{\partial x_i}\right) - \frac{2}{3}\delta_{ij}\rho\langle k\rangle \tag{4}$$

This concept assumes that the Reynolds stresses are proportional to the local mean velocity gradients and that the proportionality factor, the eddy viscosity, μ_t, is a scalar quantity, i.e., the same for all components of $\langle u_i u_j\rangle$. The eddy (turbulent) viscosity is calculated as

$$\mu_t = C_\mu \rho \frac{\langle k\rangle^2}{\langle \epsilon\rangle} \tag{5}$$

where C_μ is a constant.

The ASM can be derived by assuming that the transport of the Reynolds stresses $\langle u_i u_j \rangle$ is proportional to the transport of turbulent kinetic energy $\langle k \rangle$, i.e.,

$$C_{ij} - D_{ij} = \frac{\langle u_i u_j \rangle}{\langle k \rangle}(C_k - D_k) \tag{6}$$

where C_{ij}, D_{ij} represent the convective and diffusive transport of $\langle u_i u_j \rangle$ and C_k, D_k represent the corresponding terms for $\langle k \rangle$. The ASM representation of the Reynolds stresses, after some algebraic manipulation, can be expressed in the following explicit form:

$$\langle u_i u_j \rangle = \frac{2}{3}\delta_{ij}\langle k \rangle + \frac{\langle k \rangle}{\langle \epsilon \rangle} \frac{(1 - c_2)\left(P_{ij} - \frac{2}{3}\delta_{ij}P_k\right) + \phi_{ij,w}}{c_1 + P_k/\langle \epsilon \rangle - 1} \tag{7}$$

where P_{ij} and P_k denote the production of $\langle u_i u_j \rangle$ and $\langle k \rangle$. These production terms are exact and do not have to be modeled.

The pressure-strain correlation Φ_{ij} involves correlations between fluctuating pressure and strain rates and must be modeled. Three processes contribute to the pressure-strain correlation, one "slow" term attributable only to the interaction of fluctuating velocities ($\phi_{ij,1}$), one "rapid" term arising from the interaction of mean strain and fluctuating velocities ($\phi_{ij,2}$), and one term attributable to the effects of rigid boundaries ($\phi_{ij,w}$). Each contribution can be modeled separately [6].

At high Reynolds numbers, most of the viscous dissipation occurs at small scales. Thus, the dissipation term ϵ_{ij} can be assumed to be isotropic, so that the same amount of energy is dissipated in each energy component $\langle u_i^2 \rangle$, written as

$$\epsilon_{ij} = \frac{2}{3}\langle \epsilon \rangle \delta_{ij} \tag{8}$$

Finally, the model is closed by solving the transport equations for the turbulent kinetic energy and its dissipation rate using the exact expression for the production term including the Reynolds stresses. The diffusive terms consisting of the eddy viscosity are replaced with the more general relations:

$$(\mathrm{DIFF})_k = \frac{\partial}{\partial x_j}\left(\mu\frac{\partial \langle k \rangle}{\partial x_j} + c_s\,\rho\langle u_i u_j \rangle \frac{\langle k \rangle}{\langle \epsilon \rangle}\frac{\partial \langle k \rangle}{\partial x_i}\right) \tag{9}$$

$$(\mathrm{DIFF})_\epsilon = \frac{\partial}{\partial x_j}\left(\mu\frac{\partial \langle \epsilon \rangle}{\partial x_j} + c_{\epsilon 3}\,\rho\langle u_i u_j \rangle \frac{\langle k \rangle}{\langle \epsilon \rangle}\frac{\partial \langle \epsilon \rangle}{\partial x_i}\right) \tag{10}$$

NEAR-WALL TREATMENT: TWO-LAYER MODEL

A two-layer model combines the actual high Reynolds number turbulence model with a simpler, but more reliable one-equation model to accurately resolve

the flow near a solid wall. The model separates the flow field into an outer region, where the viscous effects are small, and an inner region, where the viscous effects cannot be neglected. In the outer region, where the turbulent Reynolds number is high, the transport equations for all the dependent variables are solved as usual. The viscous-affected inner region, which includes the sublayer, the buffer layer, and part of the fully turbulent layer, is resolved with the one-equation model. In this inner region the dissipation rate $\langle \epsilon \rangle$ is not determined from a transport equation but from a prescribed length-scale distribution. Since the ASM is not valid in this inner region, the Reynolds stresses are computed using the Boussinesq assumption, i.e., Eq. (4). The one-equation model chosen in this investigation is that proposed by Norris and Reynolds [7]. The expression for the eddy viscosity in the inner region ν_t is given as

$$\nu_t = c_\mu \langle k \rangle^{1/2} l_\mu \tag{11}$$

and $\langle \epsilon \rangle$ is determined from

$$\langle \epsilon \rangle = \frac{\langle k \rangle^{3/2}}{l_\epsilon} \tag{12}$$

Close to a wall, the turbulent energy $\langle k \rangle$ decreases, owning to the damping of the turbulent stresses, and hence, the eddy viscosity ν_t goes to zero. The damping of the eddy viscosity in this inner region is affected by a reduction of l_μ, owing to an exponential function similar to the van Driest damping function used in the mixing length theory. The Norris-Reynolds model employs the following expression of l_μ:

$$l_\mu = C_l n \left[1 - \exp\left(- \frac{\mathrm{Re}_n}{A_\mu} \right) \right] \tag{13}$$

where n is the normal distance from the wall. The turbulent Reynolds number Re_n is given as

$$\mathrm{Re}_n = \frac{\langle k \rangle^{1/2} n}{\nu} \tag{14}$$

which, in contrast to the original van Driest function, does not involve the friction velocity u^* and, hence, is valid also in cases with separated flows. The constant C_l is chosen as

$$C_l = \kappa C_\mu^{-3/4} \tag{15}$$

where C_μ is the same constant as in the standard k-ϵ model ($= 0.09$) and κ is the von Kárman constant, which is somewhat different for different modelers. The damping constant A_μ was determined from numerical tests and set to $A_\mu = 50.5$

[4]. The length scale l_ϵ in the expression for the dissipation rate (Eq. (12)) is given as

$$l_\epsilon = \frac{C_l n}{1 + 5 \cdot 3/\mathrm{Re}_n} \tag{16}$$

The one-equation model in the inner region must be matched with the high Reynolds number model in the outer region at some location in the flow. This location should be placed in a region where the viscous effects have become negligible. There are different ways of doing this. In this study, the matching took place where the damping function in the length-scale relation (Eq. (13)), i.e., the expression in brackets, has a value close to unity, which means that the viscous effects are small. For the present calculations a value of 0.95 was chosen.

BOUNDARY CONDITIONS

Inlet. The inlet was located two slot heights upstream of the rear edge of the lip. Mean velocities, velocity fluctuations, and temperature were set according to the experiments. The dissipation rate was calculated from the expression in Eq. (12), and the turbulent kinetic energy was calculated as

$$k = \frac{1}{2}\left(\overline{u^2} + \overline{v^2} + \overline{w^2}\right) \tag{17}$$

Outlet. The exit velocity was set according to global mass balance between the inlet and outlet, and a zero streamwise gradient was imposed for the remaining variables.

Symmetry. A zero gradient was imposed for all variables except for the V velocity, which was set to zero.

Blockage. A blocked region is situated inside the lip, and all quantities there were set to zero, except for the pressure and the temperature, which were extrapolated from the interior flow field.

Walls. The Norris-Reynolds one-equation model was used near the walls. On the walls, all quantities were set to zero except for the pressure and temperature, for which the gradients normal to the wall were set to zero.

CALC-BFC CODE

Basics

In this report a finite volume computer program, CALC-BFC (boundary-fitted coordinates), for three-dimensional complex geometries has been used. A detailed description of the code is given in Ref. [8], and some of its main features are briefly discussed below.

The SIMPLEC solution algorithm [9] is used, and the program uses Cartesian velocity components, collocated variables situated in the middle of the control volume, and linear interpolation when a variable is needed at a face of the control

volume. The convective terms are discretized using both a hybrid upwind/central differencing scheme, as well as a bounded scheme of second-order accuracy by van Leer [10]. The diffusive terms are discretized using central differences, which are of second-order accuracy. For the time derivatives a second-order-accurate scheme, referred to as the Crank-Nicolson scheme, as been used. All these schemes, except for that by van Leer (discussed below) are described in Ref. [9].

When using collocated variables instead of a staggered-grid arrangement for the velocities, special care must be taken when the velocities are interpolated from the nodes to the control volume faces in order to avoid nonphysical oscillations. This is due to the weak coupling between the velocity component at the face and the corresponding pressure gradient. Rhie and Chow [11] solved this problem.

Van Leer Scheme

For steady state flows, the van Leer scheme [10] proceeds as follows. First, identify the upstream (U), downstream (D), and centrally located (C) nodes for each cell face on the basis of the sign of the cell face velocity.

Thus, referring to Figure 2, if $U_{i+1/2,j}$ is positive, set $\Phi_U = \Phi_{i-1,j}$, $\Phi_D = \Phi_{i+1,j}$, and $\Phi_C = \Phi_{i,j}$. Then, if

$$|\Phi_D - 2\Phi_C + \Phi_U| \geq |\Phi_D - \Phi_U| \tag{18}$$

set

$$\Phi_{i+1/2,j} = \Phi_C \tag{19}$$

Otherwise, set

$$\Phi_{i+1/2,j} = \Phi_C + \frac{(\Phi_D - \Phi_C)(\Phi_C - \Phi_U)}{(\Phi_D - \Phi_U)} \tag{20}$$

This scheme is a first-order upwind scheme with a correction term that gives second-order accuracy. All the momentum equations, as well as the turbulent

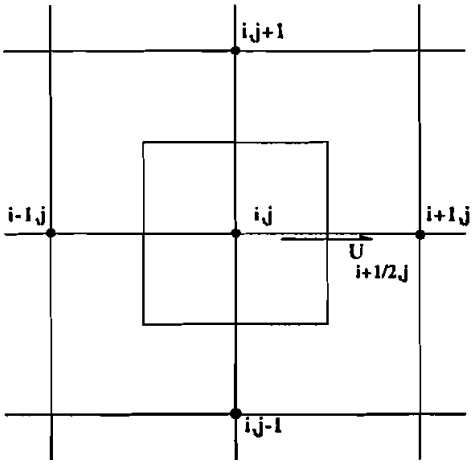

Figure 2. Grid geometry.

equations, are solved by the van Leer scheme. This bounded scheme prevents occurrence of negative values of k and ϵ. Such values are not only unrealistic, but destabilize the turbulence equations and prevent the solution from converging.

RESULTS AND DISCUSSION

The calculations of two-dimensional turbulent flow have been carried out for two different lip-to-slot ratios ($t/s = 0.1, 1.0$) and for two different velocity ratios ($M = 1.0, 1.5$). The results are presented in more detail in Ref. [12]. The bulk temperature in the slot, T_s was approximately 40°C, and in the free stream the temperature T_g was 23–29°C. An assumption was made that the temperature had no influence on the velocity field, since the temperature differences are quite small. Hence the buoyancy effects should be negligible in comparison with the convection terms.

In order to minimize the number of grid points, an expanded grid was used in which the resolution was high in those regions where the gradients were expected to be great. The outlet boundary condition was set 50–80 slot heights downstream of the lip in order to be sure that the vortex shedding has dissipated, and hence the streamwise gradients could be set to zero. The upper boundary was set 12 slot heights over the wall in order to be able to accept a symmetry condition. The grid points within the lip are blocked, and hence all quantities except for the dissipation rate and temperature are set to zero. The grid near the lip is shown in Figure 3.

Steady Calculations: Case $t/s = 1.0$

The calculations in this case were performed at two different Reynolds numbers (12,550 and 18,950) based on the slot height s and the mean velocity in

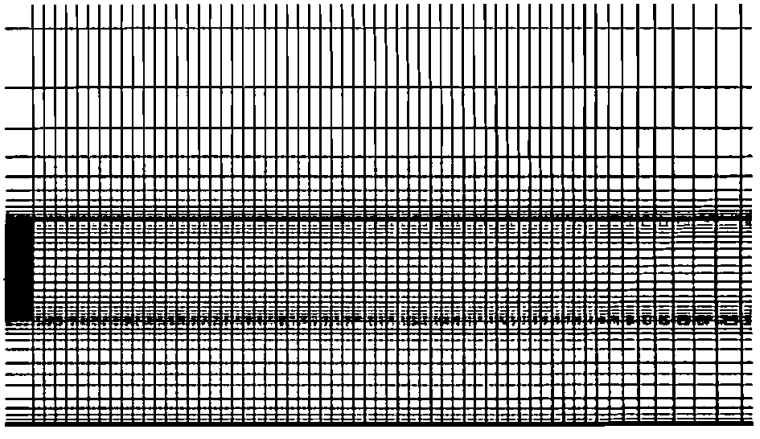

Figure 3. Grid near the lip, which is defined by the dark area.

the slot U_s. In this case there was no difference in the results between the use of the hybrid and the van Leer scheme. The lip itself causes little disturbance, and the flows will interact as two merging shear layers and not as a turbulent wake. For this case, the downstream effects of the lip are primarily due to the difference in velocity between the two flows. Steady solutions were obtained no matter which of the turbulence models was used. The total grid consisted of 190 × 80 grid points. It should be mentioned that no calculations were made using a finer grid, but the fact that the same results were obtained with the hybrid and the van Leer scheme indicates that the calculations were grid independent.

Since single hot-wire equipment was used in the experimental study by Boman and Olsson [1], the measured velocity has contributions from the components in both the x- and y-directions. The calculated velocities U in Figure 4*a* are therefore the absolute values. The agreement is good between calculations and measurements considering the mean velocities for both turbulence models.

The dimensionless mean temperatures are shown in Figure 4*b*, and the agreement between measurements and calculations is good in both the free stream and the mixing layer. The mean flow does not seem to penetrate much into the slot flow, which results in a high film cooling effectiveness near the wall. This low mixing of the flows is probably due to the fact that the thin lip creates very little vortex shedding and, hence, the periodic fluctuation, which is important for the mixing process, is small. Since it was assumed that the temperatures did not affect the velocities, the only differences in the transport equation for the velocity and the temperature are the expression of the diffusion term and the fact that no source terms appear in the equation. The diffusion term in the temperature equation was calculated using a Boussinesq approximation for both the k-ϵ model and the ASM as

$$\frac{\partial}{\partial x_i}\left[\left(\frac{\mu}{\sigma}+\frac{\mu_t}{\sigma_t}\right)\frac{\partial\langle T\rangle}{\partial x_i}\right] \tag{21}$$

where σ and σ_t are the laminar and the turbulent Prandtl numbers. The value of the turbulent Prandtl number was set to 0.9 in the near-wall region and 0.5 elsewhere. The latter value has been found to be appropriate for plane jets, wakes, and mixing layers [15]. At the wall ($y/s = 0$), the results come together in a single point at θ around unity in the region near the lip, but θ decreases for higher x/s. The potential core region prevails as long as there is a clear velocity maximum and a turbulence minimum in the region $y/s \leq 1$. The calculated profiles in the last position indicate that the vertical mixing is too large in the calculations. This is probably due to the coarse grid at this position, which in turn, leads to numerical diffusion and the profiles being smeared out. Except for the last position considered, the film cooling effectiveness at the wall is generally well predicted.

Considering the velocity fluctuations, when the ASM was used, the absolute value of the fluctuation was taken as

$$u' = u_{\text{abs}} = [\langle u^2\rangle + \langle v^2\rangle]^{1/2} \tag{22}$$

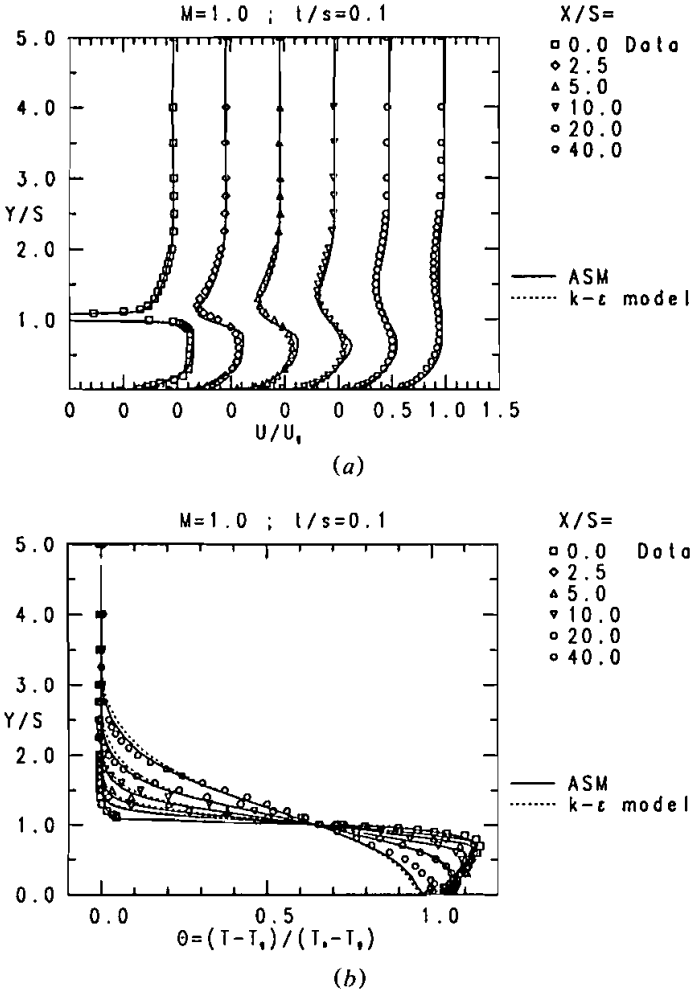

Figure 4. (*a*) Mean velocity profiles, $M = 1.0$, $t/s = 0.1$. (*b*) Dimensionless temperature profiles, $M = 1.0$, $t/s = 0.1$.

and when the k-ϵ model was used, it was calculated assuming isotropic turbulence, as

$$u' = u_{\text{abs}} = \left(\frac{4}{3}\langle k\rangle\right)^{1/2} \tag{23}$$

It was seen that the fluctuations obtained form the k-ϵ model were generally equal to those obtained from the ASM, but both models resulted in higher values as compared with the data [12]. The level of fluctuations was highest at the slot exit on the lower side of the lip, but further downstream it decreased and the profiles filled out. The poor agreement between calculated and measured fluctuations close

to the wall and on the lower side of the lip may be explained by the fact that the stresses varied over time. Another uncertainty about the fluctuations arises from the injection arrangement (see Ref. [1]), where there must be curvature effects convected from the sharply curved channel to the plane inlet, which will have a stabilizing effect on the fluctuations. However, the principal form of the profiles according to local minimums and maximums was in quite good agreement with the measurements. In the near-wall region, where both the ASM and the k-ϵ model are invalid, the stresses were calculated using the eddy viscosity assumption in Eq. (4), where the turbulent viscosity was calculated using the expression in the Norris-Reynolds one-equation model, Eq. (11).

Unsteady Calculations: Case $t/s = 1.0$

The calculations for this case (Re_s = 12,400) resulted in unsteady motions. This unsteady behavior of the flow is due to vortex stretching, with vortices alternatively shedding from the upper and lower edges of the lip, forming a periodic von Karman vortex sheet behind it. Vortex shedding is a periodic unsteady flow phenomenon that occurs frequently behind relatively slender, bluff structures and is therefore of great practical importance. In Figure 5*a* the instantaneous velocity field behind the lip is shown. The vortex at the lower edge is convected downstream, and at the upper edge a new vortex is beginning to form. To illustrate the periodicity of the flow, the V velocity at a location in the wake is presented as a function of time in Figure 5*b*. It can be seen that after a while, an almost perfect periodicity exists with a well-defined frequency.

In Figure 6 the pressure contours at different times during a whole cycle are shown. At the lower edge of the lip, a vortex has just been created and is convected downstream as time increases. During its transport, it will continuously lose vorticity, which can be seen by the increasing distance between the isobars in the vortex. All the unsteady calculations presented here were calculated using the Crank-Nicolson time discretization scheme, and both the hybrid upwind/central differencing scheme and the scheme of van Leer were used for the convection terms. The grid consisted of 190 × 144 grid points. The total time of a cycle was almost 2.5 ms and has been divided into approximately 90 time steps of $\Delta\tau = 25\mu$s in the calculations, which gave a Strouhal number Sr of

$$\mathrm{Sr} = \frac{f\tau}{U_s} \approx 0.22 \tag{24}$$

At high Reynolds numbers, three-dimensional stochastic turbulent fluctuations are superimposed on the periodic unsteady motion. The instantaneous velocity component U_i is separated into time-mean velocity components $\overline{U}_i$, periodic fluctuating components $\tilde{U}_i$ (together called phase averaged, $\langle U_i \rangle$), and turbulent fluctuating components u_i, i.e.,

$$U_i = \overline{U}_i + \tilde{U}_i + u_i = \langle U_i \rangle + u_i \tag{25}$$

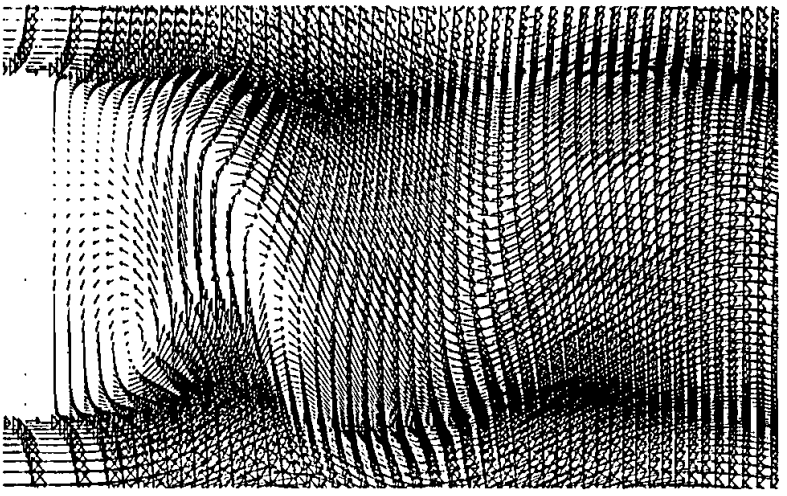

(*a*)

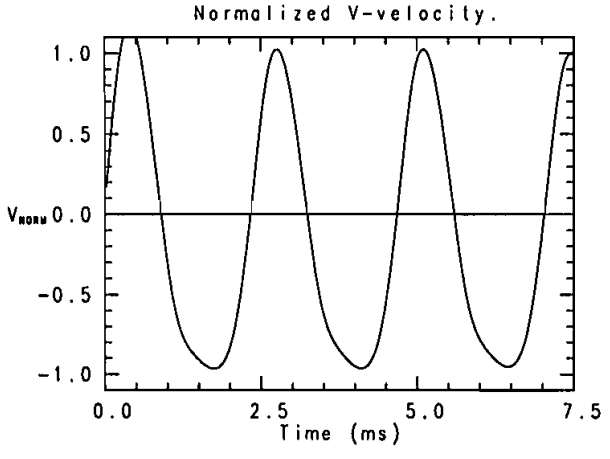

(*b*)

Figure 5. (*a*) Instantaneous velocity field behind the lip, $M = 1.0$, $t/s = 1.0$. (*b*) Normalized V velocity at $x/s \approx 2.0$, $y/x \approx 2.0$, $M = 1.0$, $t/s = 1.0$.

where $\langle U_i \rangle$ is the velocity resolved by the numerical method.

The time-averaged mean velocities in the calculations are shown in Figure 7. With the use of the k-ϵ model, the results obtained using the van Leer scheme are in considerably better agreement with the measurements than those obtained by using the hybrid upward/central differencing scheme. This is equivalent to the results *not* being grid independent. One conclusion from Figure 7 is that the ASM predicts the flow field better than the k-ϵ model. However, when the van Leer scheme is used, one must say that both models are capable of predicting the flow.

From Figures 8 and 9 it can be seen that the k-ϵ model leads to heavily overpredicted turbulent fluctuations in the wake region. This overprediction of

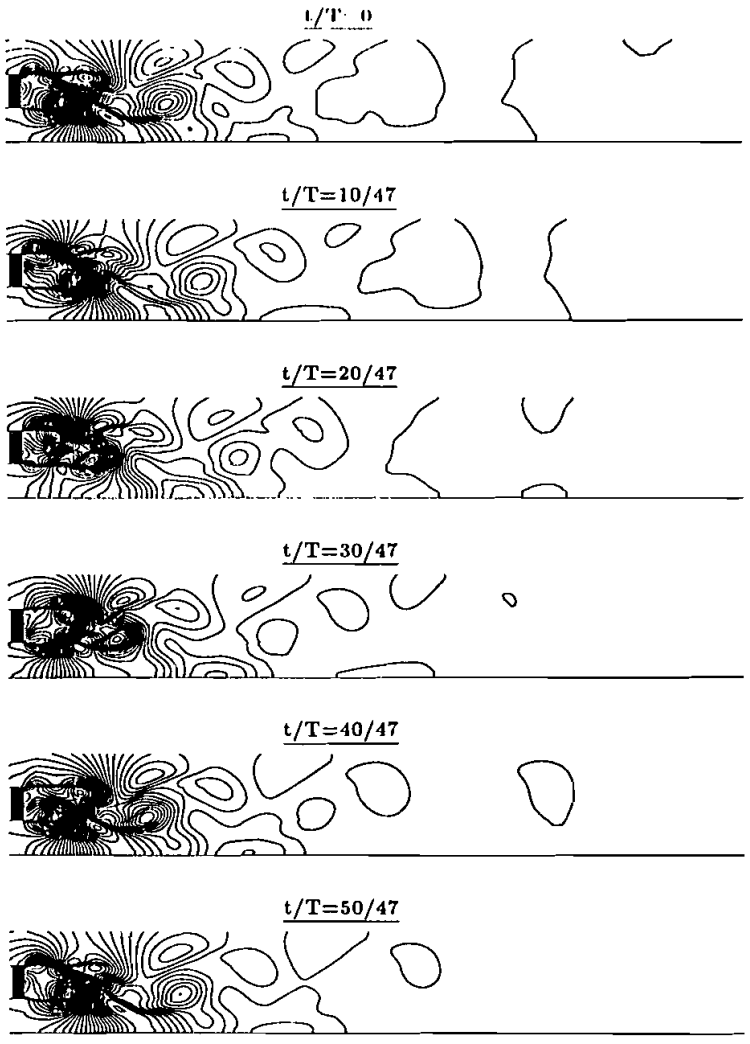

Figure 6. Pressure contours at different times during one cycle.

turbulent kinetic energy results in excessive eddy viscosity, which damps the periodic fluctuations. The turbulent fluctuations obtained from the ASM are smaller than the measurements. This is physically correct, since the measured values are the *sum* of the absolute periodic and turbulent fluctuations. The corresponding calculated fluctuations time-averaged over a whole cycle $\overline{u_{\mathrm{TOT}}}$ are computed as

$$\overline{u_{\mathrm{TOT}}} = \frac{1}{n} \sum_{m=1}^{n} \left[\left| \left(\langle U \rangle^2 + \langle V \rangle^2 \right)^{1/2} - \overline{\left(\langle U \rangle^2 + \langle V \rangle^2 \right)^{1/2}} \right| + u_{\mathrm{abs}} \right]_m \tag{26}$$

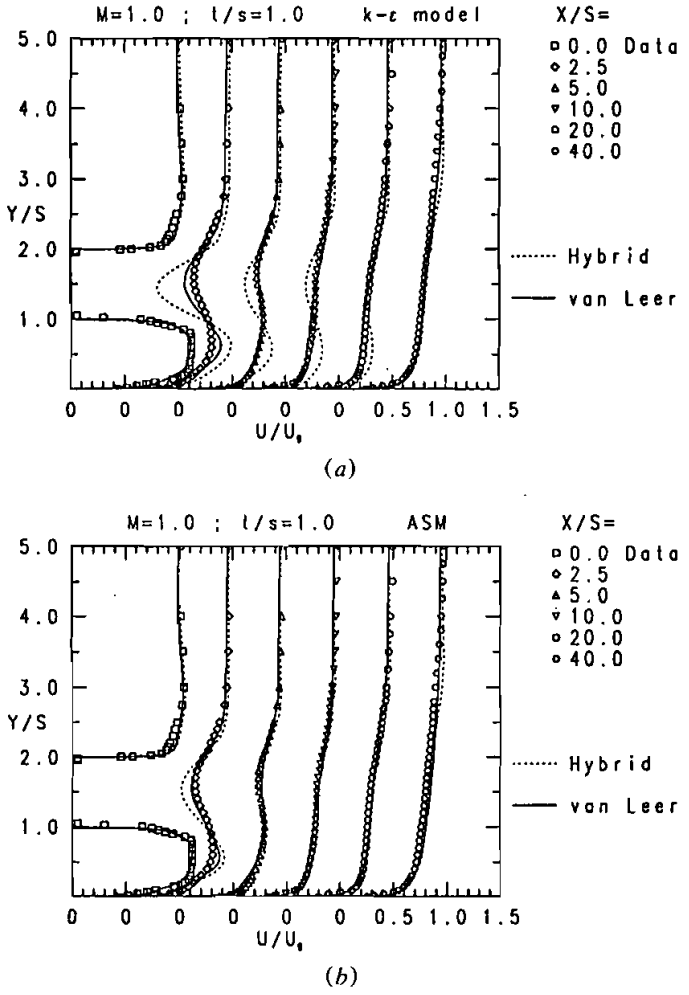

Figure 7. (*a*) Time-averaged mean velocity profiles using the (*a*) k-ϵ model and (*b*) ASM.

where n is the number of time steps during one cycle. It can be seen from Figure 8 that the contribution from the periodic fluctuations is quite high near the lip. Further downstream the periodic contribution decreases, indicating that the strength of the vortex sheet decreases and that the transport of mean momentum is less affected by the periodic fluctuations. The fluctuations in the free stream are in better agreement with the measurements when the van Leer scheme is used, indicating that the vortex shedding is better predicted and stronger than in the case where the hybrid scheme is used. The reason is that the van Leer scheme is less diffusive (second-order accurate) compared with the hybrid scheme (first-order accurate). This stronger vortex shedding gives a better vertical mixing between the two flows.

It is interesting to study whether the transport of mean momentum is most affected by turbulent fluctuations or by the periodic fluctuations owing to the

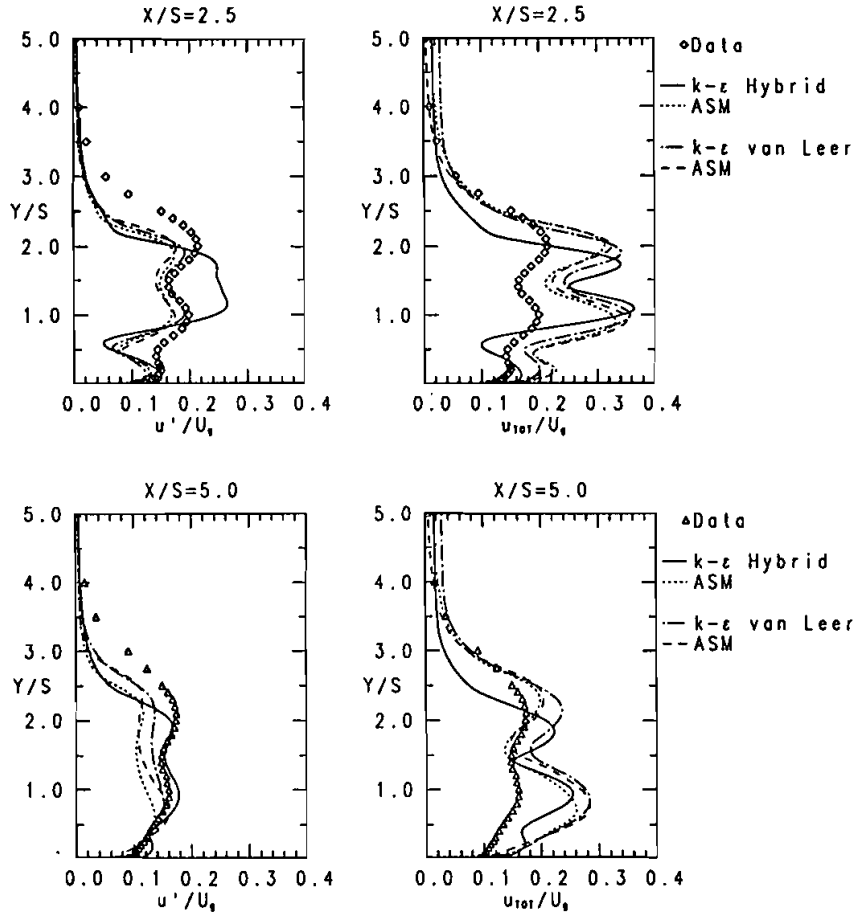

Figure 8. Turbulent $(\overline{u'}/U_g)$ and total $[\overline{(u' + \tilde{U})}/U_g]$ velocity fluctuations for $x/s = 2.5$ and 5.0.

vortex shedding. Using Reynolds decomposition to divide the instantaneous velocity component into a mean part and a fluctuating part gives an expression for the unsteady transport equation for the phase-averaged velocity component $\langle U_i \rangle$:

$$\rho \frac{\partial \langle U_i \rangle}{\partial \tau} + \rho \frac{\partial}{\partial x_j}\left(\langle U_i \rangle \langle U_j \rangle\right) = -\frac{\partial \langle P \rangle}{\partial x_i} + \frac{\partial}{\partial x_i}\left[\mu\left(\frac{\partial \langle U_i \rangle}{\partial x_j} + \frac{\partial \langle U_j \rangle}{\partial x_i}\right) - \rho \langle u_i u_j \rangle\right]$$

Replacing $\langle U_i \rangle$ with the expression in Eq. (25) and performing a second time averaging over a whole cycle on the expression above gives the following equation:

$$\rho \frac{\partial}{\partial x_j}\left(\overline{U_i}\,\overline{U_j}\right) = -\frac{\partial \overline{P}}{\partial x_i} + \frac{\partial}{\partial x_j}\left[\mu\left(\frac{\overline{\partial U_i}}{\partial x_j} + \frac{\overline{\partial U_J}}{\partial x_I}\right) - \rho\overline{u_i u_j} - \rho\overline{\tilde{U}_i \tilde{U}_j}\right] \tag{27}$$

where $\rho\overline{u_i u_j}$ and $\rho\overline{\tilde{U}_i \tilde{U}_j}$ are the stresses due to turbulent and periodic fluctuations, respectively. In Figure 10, the time-averaged shear stresses by the periodic fluctua-

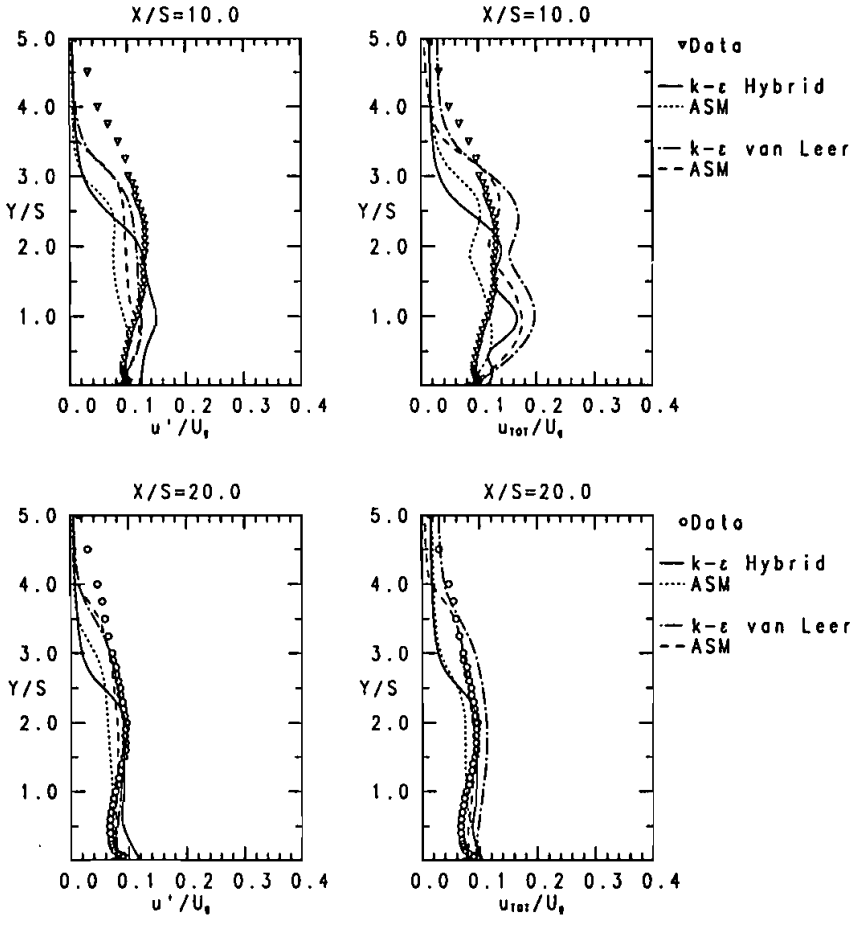

Figure 9. Turbulent $(\overline{u'}/U_s)$ and total $[\overline{(u' + \tilde{U})}/U_s]$ velocity fluctuations for $x/s = 10$ and 20.

tions $(\overline{\tilde{U}\tilde{V}})$ are compared with those obtained from the turbulent fluctuations $(\overline{uv})$ using the van Leer scheme. The shear stresses achieved by the mean flow periodicity are greater than the Reynolds shear stresses and can be interpreted as the strength of the vortex shedding. These shear stresses by the mean flow are calculated as

$$\overline{\tilde{U}\tilde{V}} = \frac{1}{n} \sum_{m=1}^{n} \left[(\langle U_m \rangle - \bar{U})(\langle V_m \rangle - \bar{V}) \right] \tag{28}$$

and when the k-ϵ model is used, the turbulent shear stresses are calculated according to the Boussinesq assumption:

$$\overline{uv} = -\frac{\mu_t}{\rho} \left(\frac{\partial \langle U \rangle}{\partial y} + \frac{\partial \langle V \rangle}{\partial x} \right) \tag{29}$$

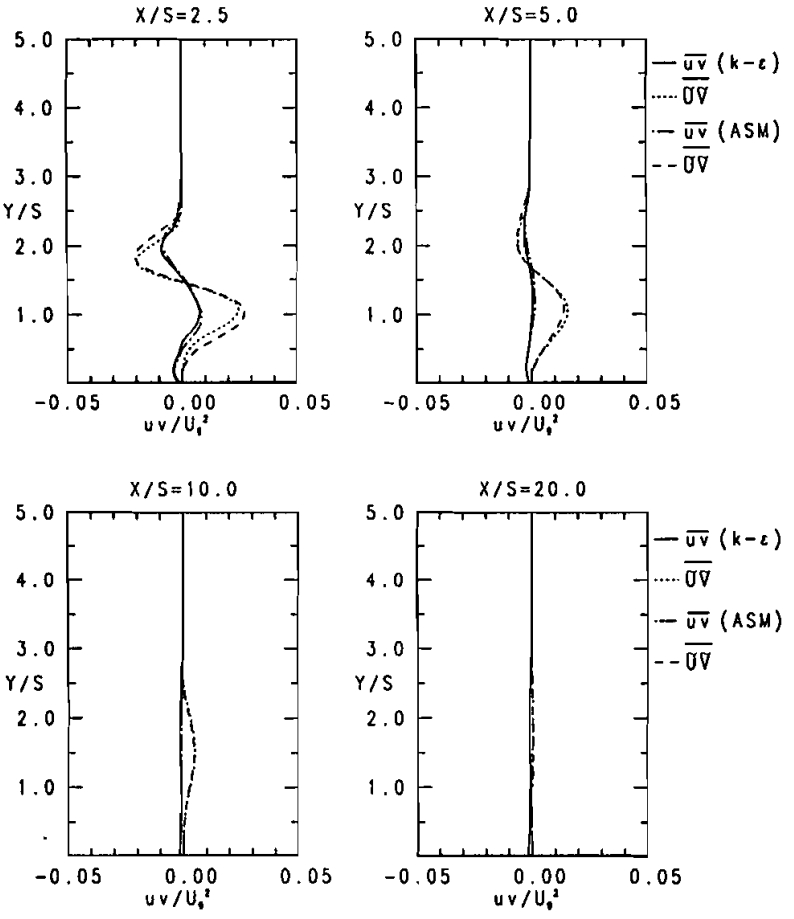

Figure 10. Mean($\overline{\tilde{U}\tilde{V}}$) and turbulent ($\overline{uv}$) shear stresses.

In Figure 11 the time-averaged dimensionless mean temperature profiles are shown, and it can again be noted that the van Leer scheme results in better mixing between the flows, owing to the stronger periodicity. Considering the same discretization scheme and comparing the turbulence models, it can be seen that in the ASM case, the profiles are a little more smeared out and better predicted than those obtained in the k-ϵ case. This is a result of the higher momentum exchange from the mean flow in the y direction, and hence the main and slot flows are more mixed when the ASM is used. In the near-wall region the calculated film-cooling effectiveness is generally too high, which indicates that the flow in the free stream does not penetrate far enough into the slot flow, which means that the calculated vortex shedding is too weak. Further downstream, the film cooling effectiveness is decreased, owing to the increased mixing of the flows, which acts to destroy the "heating" film. It should be noted that in the calculations as well as in the measurements, the wall was assumed to be adiabatic and that the "hot" flow was in the slot.

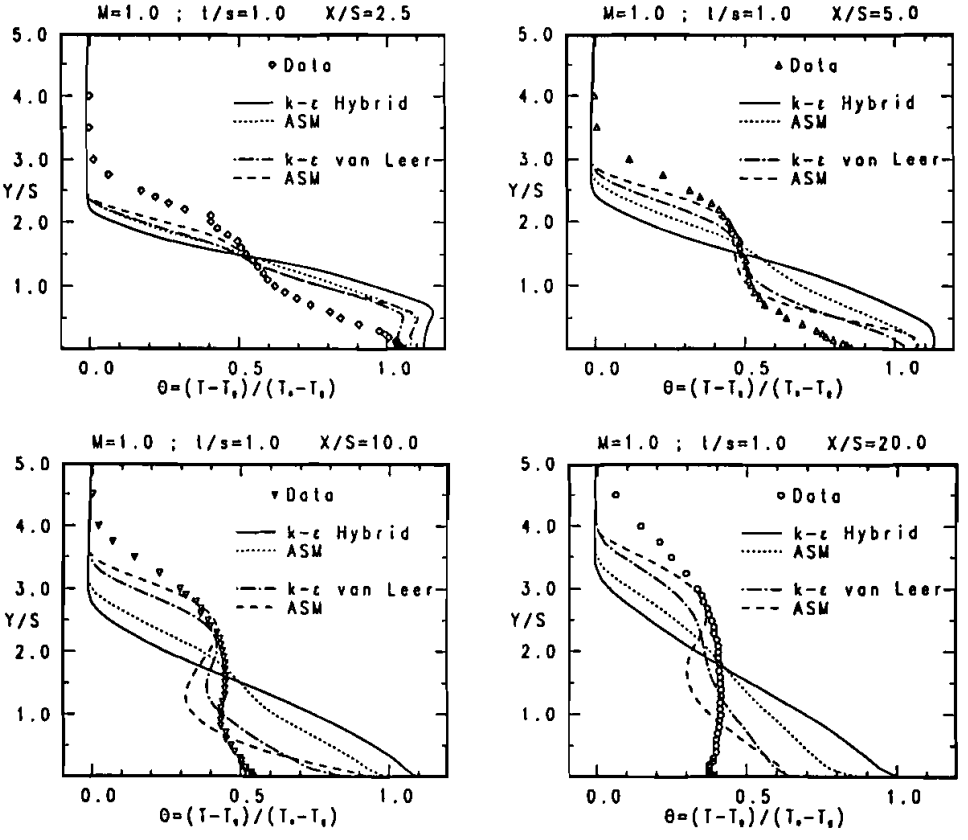

Figure 11. Dimensionless temperature profiles at $x/s = 2.5$ and 5.0.

There were some difficulties in comparing the calculations with the measurements, since the temperature in the free stream varied from day to day during the measurements. This means that the temperature in the free stream during the measurement of a temperature profile at a downstream location varied from the free stream temperature during the measurements at another location. The predicted temperature fields were very sensitive to how the diffusive term in the transport equation for the temperature was modeled. When the k-ϵ model was used, it was taken from the eddy viscosity assumption, as mentioned. In the calculations using the ASM the diffusion term was approximated by the following gradient-type expression [16]:

$$-\langle u_i\theta\rangle = C_\theta \frac{\langle k\rangle}{\langle \epsilon\rangle}\langle u_i u_j\rangle \frac{\partial\langle T\rangle}{\partial x_j} \tag{30}$$

where the constant C_θ was taken as 0.11.

Figure 12*a* shows the instantaneous isolevels of the temperature behind the lip. The penetration of the cold flow above the lip into the hot flow increases in the beginning and then decreases owing to the damping of the vortex shedding.

Figure 12*b* displays the distribution of the time-averaged $\overline{U}$ velocity along the centerline of the wake, revealing that the k-ϵ model produces a longer separation region than the ASM and hence the velocity in the wake region is lower. This is due to the fact that the vortex shedding is weaker in the k-ϵ case, which results in less periodic fluctuations and hence lower time-averaged velocities in the wake.

The variation of the normalized temperature and velocity components along the centerline of the wake during one cycle is shown in Figure 13. As can be seen in the figure (x/s = 10), the temperature at the centerline is low most of the time during one cycle. This means that the cold flow passes through this region most of the time. The variations of the velocity component normal to the wall $\langle V \rangle$ and the temperature are not symmetric with respect to their mean values. This is due to the presence of the wall, which acts to damp the low peaks in the cyclic variations. This is also seen in Figure 5*b* (to a smaller extent, as the point considered is located further away from the wall), where the negative peaks are slightly smeared out. A general conclusion is that the temperature is high when both the velocity components are positive, which means that the flow has a direction coming from the slot

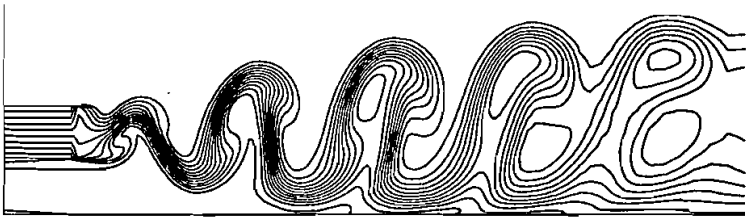

(*a*)

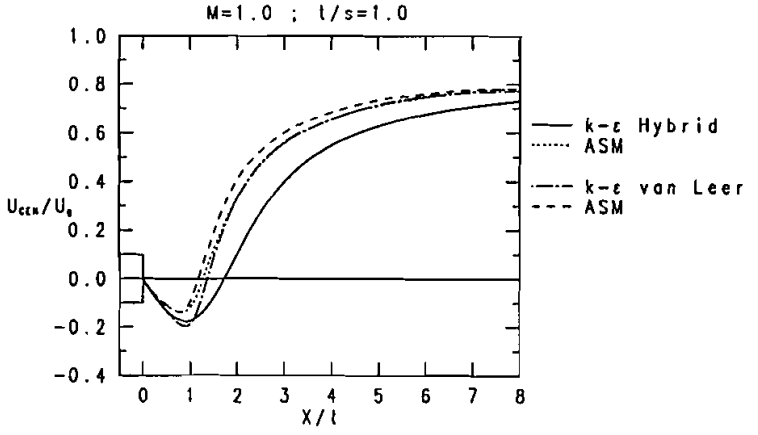

(*b*)

Figure 12. (*a*) Isolevels of the instantaneous temperature field. (*b*) Time-averaged streamwise velocity along the centerline of the wake.

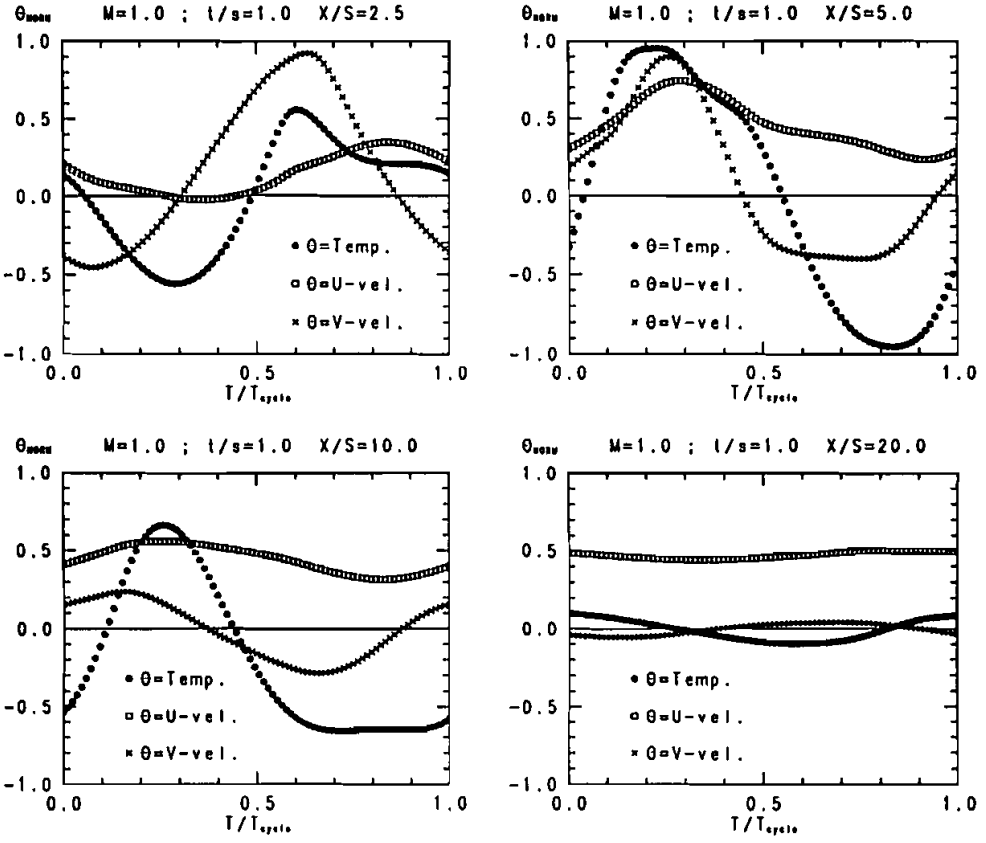

Figure 13. Temperature and velocity variation along the centerline of the wake during one cycle.

region. It can be seen in Figure 13 that the positive peak in the temperature profile at $x/s = 2.5$ at time $T/T_{\text{cycle}} = 0.6$ appears at $x/s = 5.0$ in the following time cycle at time $T/T_{\text{cycle}} = 0.2$.

CONCLUDING REMARKS

The two-dimensional, unsteady (and steady), turbulent calculations of the wake flow in a film-cooling arrangement have been carried out for different lip-to-slot ratios and flow ratios. There will always be an unsteady wake flow behind the lip, but when the lip is thin ($t/s = 0.1$), the periodic fluctuations in the wake are small and do not much affect the flow. The main effect of the lip in this case is the difference in velocity between the flows in the slot and the free stream. This means that a steady calculation of the problem can predict the flow quite well, and for this case, both turbulence models used in this study predicted the flow very well.

As the lip thickness increases ($t/s = 1.0$), the effect of the unsteady wake flow on the global flow pattern becomes considerable, and stationary solutions of

these cases cannot be obtained. Hence, unsteady calculations are required to predict the flow field properly. Owing to this unsteady wake flow, the periodic fluctuations increase the mixing of the flows in the slot and in the free stream, and the film cooling effectiveness is decreased. Eddy viscosity calculations with the k-ϵ model result in velocities that are too low in the wake and in considerable differences in the observed level of the total fluctuations (periodic + turbulent) measured in the wake. The simulated periodic fluctuations due to the vortex sheet are underpredicted compared with experiments. This affects the global flow pattern, as the present calculations show that these fluctuations contribute considerably to the time averaged momentum transfer. The k-ϵ model apparently produces excessive eddy viscosity, which damps the periodic fluctuations, and hence the mixing between the flows becomes too low. In these unsteady cases it is well known that it is important to take adequate account of production and pressure-strain effects of the individual Reynolds stresses in order to obtain good agreement. It is obvious that for the vortex shedding flows in these cases, the isotropic eddy viscosity concept is invalid in parts of the flow domain. Finally, the following conclusions can be drawn.

- Both turbulence models predict the flow field quite correctly when the lip is thin ($t/s = 0.1$) and no streamline curvature effects are present. Calculated velocities and temperatures at different locations downstream are very well predicted.
- When the lip thickness increases ($t/s = 1.0$) and hence the flow becomes unsteady, it is of great importance that a fine grid in space (or a higher order scheme) be used to achieve good agreement with experiments. When a quite coarse grid was used at the beginning of the calculations, an unphysical *steady* solution was obtained owing to the great numerical diffusion, which is significant at coarse grids.
- In the unsteady cases, where streamline curvature effects are present, the eddy viscosity concept in the k-ϵ model is not valid, and the anisotropic behavior of the turbulence is better predicted by the ASM. Best predictions are obtained by using the ASM in combination with van Leer's differencing scheme of second order accuracy. The calculated fluctuations are generally overpredicted in the region near the lip. The calculated film-cooling effectiveness at the wall is too large, indicating that the penetration of the cold flow in the free stream into the slot is too weak, and hence the calculated vortex shedding is weaker than in the experiments.
- It is concluded that the lateral transport of mean momentum is affected more by the vortex shedding than by turbulence.

REFERENCES

1. U. Boman and E. Olsson, The Influence of High Lip-to-Slot-Thickness on Film Cooling Effectiveness, 19th Int. Congress on Combustion Engines, No. 611, Florence, Italy, 1991.
2. B. E. Launder and W. Rodi, The Turbulent Wall Jet—Measurements and Modeling, *Annu. Rev. Fluid Mech.*, vol. 15, pp. 429–459, 1983.
3. S. C. Kacker and J. H. Whitelaw, Predictions of Wall-Jet and Wall-Wake Flow, *J. Mech. Eng. Sci.*, vol. 12, no. 6, pp. 404–419, 1970.

4. W. Rodi, Experience with Two-Layer Models Combining the k-ϵ Model with a One-Equation Model near the Wall, 29th Aerospace Sciences Meeting, January 7–10, Reno, Nev., AIAA Paper 91-0216, 1991.
5. W. Rodi and G. Scheurer, Calculation of Curved Shear Layers with Two-Equation Turbulence Models, *Phys. Fluids*, vol. 26, no. 6, pp. 1422–1435, 1983.
6. J. C. Rotta, *Turbulente Strömungen*, B. G. Teubner, Stuttgart, 1972.
7. L. H. Norris and W. C. Reynolds, Turbulent Channel Flow with a Moving Wavy Boundary, Department of Mechanical Engineering, Stanford University, Stanford, Calif., Rept. FM-10, 1975.
8. L. Davidson and B. Farhanieh, CALC-BFC: A Finite-Volume Code Employing Collocated Variable Arrangement and Cartesian Velocity Components for Computation of Fluid Flow and Heat Transfer in Complex Three-Dimensional Geometries, Department of Applied Thermodynamics and Fluid Mechanics, Chalmers University of Technology, Report. 92/4, Gothenburg, Sweden, 1989.
9. S. V. Patankar, *Numerical Heat Transfer and Fluid Flow*, Hemisphere, Washington, D.C., 1980.
10. B. van Leer, Towards the Ultimate Conservative Difference Scheme: Monotonicity and Conservation Combined in a Second Order Scheme, *J. Comput. Phys.*, vol. 14, pp. 361–370, 1974.
11. C. M. Rhie and W. L. Chow, Numerical Study of the Turbulent Flow Past an Airfoil with Trailing Edge Separation, *AIAA J.*, vol. 21, pp. 1527–1532, 1984.
12. L. S. Jansson, Numerical Investigation of Steady and Unsteady Flows Comparing Turbulence Models and Different Near-Wall Models, Licentiate of Engineering Thesis, Department of Thermo and Fluid Dynamics, Chalmers University of Technology, Rept. 92/1, Gothenburg, Sweden, 1992.
13. B. E. Launder, G. J. Reece, and W. Rodi, Progress in the Development of a Reynolds Stress Turbulence Closure, *J. Fluid Mech.*, vol. 68, pp. 537–566, 1975.
14. B. J. Daly and F. H. Harlow, Transport Equations in Turbulence, *Phys. Fluids*, vol. 13, pp. 2634–2649, 1970.